# Monte Carlo studies of crumpling for Sierpinski gaskets

Edward Levinson*
*Department of Physics, Simon Fraser University, Burnaby, British Columbia, Canada V5A 1S6*
(Received 7 November 1990)

Monte Carlo simulations have been performed on tethered networks possessing the connectivity of a $b=2$ Sierpinski gasket, both with and without self-avoidance. For networks without self-avoidance, the simulations are found to be in reasonable agreement with the theoretical prediction, $\nu_0 \approx 0.3685$, and independent of the embedding dimension $d$. For networks with self-avoidance, the simulations give clear evidence for crumpling. The measured value for $\nu$ is in good agreement with the Flory theory and, to a lesser extent, the first-order $\epsilon$ expansion of an appropriately generalized Edwards model. The upper critical dimension, $d_{\mathrm{UC}}$, above which self-avoidance is irrelevant, is found to lie in the range $8 < d < 10$, which is consistent with the theoretical prediction $d_{\mathrm{UC}} \approx 8.6$. The shapes of crumpled gaskets were also measured and found to be considerably more spherical than those of polymers.

## I. INTRODUCTION

In recent years tethered membranes have emerged as useful models for simulating the thermodynamics of certain types of membranes and, especially, for addressing the question of the existence of a crumpling transition.[1–5] They are, in many respects, analogous to the random walks used for studying polymers. However, unlike self-avoiding (SA) random-walk simulations, whose results are in good agreement with experimental evidence, simple theoretical predictions[6] (Flory calculations), and more sophisticated theoretical analyses ($\epsilon$ expansions of the Edwards model[7] and real-space renormalization-group arguments[8]), the results of SA tethered-membrane simulations do not agree with Flory calculations,[2] real-space renormalization-group calculations,[9] or $\epsilon$ expansions[10] of a generalized Edwards model. Specifically, for SA membranes embedded in a three-dimensional space ($d=3$), the Flory theory predicts $\nu=\frac{4}{5}$, real-space renormalization arguments give $\nu \approx 0.8$, and the $\epsilon$ expansion gives $\nu=0.536+O(\epsilon^2)$. This latter value violates the lower bound $\nu=\frac{2}{3}$ imposed by a simple geometric argument[2,11] ($\nu$ determines how the radius of gyration $R_g$ scales with the intrinsic length $L$ of the system; i.e., $R_g \sim L^{\nu}$). On the other hand, the results of several different simulations[4,5] indicate $\nu \approx 1.0$.[12] Furthermore, direct measurements of an appropriate shape parameter (described in detail below) indicate that membranes become increasingly flat as the thermodynamic limit is approached. Although there has been some disagreement over the validity of the simulation results,[13] there is increasing evidence to indicate that they are essentially correct. We are left, therefore, with the conclusion that theoretical approaches that work quite well for polymers fail to describe even the qualitative features of membranes.

In the context of field theory, both polymers and membranes are seen as special cases of a more general (but still *homogeneous)* manifold characterized by a parameter $D$, which measures its degree of intrinsic connectivity or topological dimension. Thus, $D=1$ for polymers, while for membranes $D=2$. It is then apparent that as $D$ increases, somewhere in the regime $1 < D \leq 2$, three things must occur: (1) Renormalization-group arguments and, possibly, the $\epsilon$ expansion break down; (2) the Flory theory must cease to contain all of the essential physics needed to describe the thermodynamics properly; (3) the thermodynamic behavior of the manifold must change from crumpled to flat.

It seems worthwhile to study the connections between these three points and the reasons why the theory breaks down in the first place. Ideally, one would like to compare the results of simulations with theoretical calculations for arbitrary $D$ and to look for discrepancies. Unfortunately, it is not clear how to simulate such manifolds. To overcome this difficulty, a model is needed that is amenable to simulation and theoretical calculations and which interpolates between polymers and membranes. In this article, I propose regularly connected fractal networks for this purpose. Although not homogeneous, these networks are characterized by a spectral dimension[14] $d_S$, which is completely determined by the intrinsic connectivity of the network, and, in many ways, plays the role of $D$ (see Sec. II). As a result, they are amenable to both Flory theory calculations and $\epsilon$ expansions. They are also straightforward to simulate. The remainder of this article is concerned with the comparison between Flory theory calculations, $\epsilon$ expansions, and simulations for a particular model: a network with the connectivity of a $b=2$ Sierpinski gasket.[15] As we shall see, the SA version does, in fact, crumple; the Flory theory is reasonably accurate; and the $\epsilon$ expansion gives modest results for $d=3$ but improves as $d$ approaches its upper critical dimension.

## II. THEORY

Figure 1 shows the intrinsic connectivity of the model, which is that of a $b=2$ Sierpinski gasket. For the $n$th iteration of the network, the number of vertices is

 

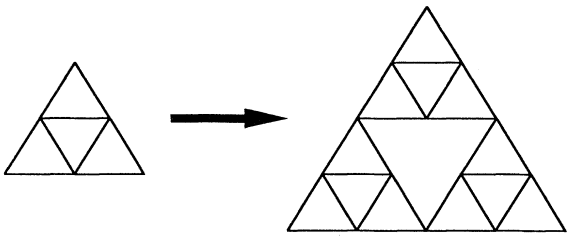


FIG. 1. Iteration process for a $b=2$ Sierpinski gasket. The value of $b$ gives the multiplication factor for the increase in the number of connections along an edge after each iteration.

$$N=\frac{3^{n+1}+3}{2} . \tag{1}$$

The lattice fractal and spectral dimensions, defined in the $n\rightarrow\infty$ limit, are, respectively,[14]

$$d_{fl}=\frac{\ln 3}{\ln 2}\approx 1.585 \tag{2a}$$

and

$$d_S=2\frac{\ln 3}{\ln 5}\approx 1.365 . \tag{2b}$$

Two versions of the model are discussed here: a phantom network, which allows the nodes to overlap, and a SA network, which does not.

*Theoretical predictions.* There exists for the phantom network a rigorous prediction for the scaling exponent $\nu$ based on a mapping between the partition functions for tethered membranes and resistor networks with the same connectivity.[2] This mapping predicts (subscript zero denotes phantom-network quantities)

$$\nu_0=\left[\frac{2-d_S}{2}\right]\frac{d_{fl}}{d_S} , \tag{3}$$

so

$$d_{f0}=\frac{d_{fl}}{\nu_0}=\frac{2d_S}{2-d_S} . \tag{4}$$

$d_{f0}$ is the Hausdorff dimension, which relates the radius of gyration to the number of vertices,

$$R_{g0}\sim N^{1/d_{f0}} . \tag{5}$$

For SA networks, a Flory theory can be constructed using a line of argument similar to the one for polymers.[6] The free energy ($v_0$ measures the excluded volume),

$$\frac{F}{k_BT}=\left[\frac{R_g}{R_{g0}}\right]^2+v_0\frac{N^2}{R_g^d} , \tag{6}$$

is minimized with respect to $R_g$ and gives

$$\nu_F=\left[\frac{d_S+2}{d+2}\right]\frac{d_{fl}}{d_S} . \tag{7}$$

Similar kinds of arguments can be made to determine the upper critical dimension $d_{\rm UC}$ above which self-avoidance is irrelevant. One such argument is to observe that $d_{f0}$ measures how much of the embedding space is filled by the fractal object. For embedding spaces with $d>2d_{f0}$, intersections between two or more portions of the network separated by large intrinsic distances will be unlikely; hence, $d_{\rm UC}=2d_{f0}$. An alternative, but related, argument is that including self-avoidance always increases $R_g$, so $\nu_0$ is a lower bound on $\nu_F$. Hence,

$$\nu_F|_{d=d_{\rm UC}}=\nu_0 . \tag{8}$$

Either way, one finds

$$d_{\rm UC}=\frac{4d_S}{2-d_S} . \tag{9}$$

Substitution of Eq. (2b) into Eq. (9) gives $d_{\rm UC}\approx 8.6$ for the $b=2$ Sierpinski gasket. This is in marked contrast to the case of homogeneous membranes[10] (i.e., $D=2$ networks) for which $d_{\rm UC}=\infty$.

Also, notice that Eqs. (3), (4), (7), and (9) reduce to the corresponding homogeneous-manifold results by simply substituting $d_S=d_{fl}=D$. In this sense $d_S$ plays the roll of an effective topological dimension.

*The Edwards model.* There have been several studies of homogeneous manifolds that have applied $\epsilon$-expansion techniques[10] to a generalized version of the Edwards model,[16]

$$\beta\mathcal{H}=\int_0^L d^Dx\left[\frac{\partial\mathbf{r}(x)}{\partial x}\right]^2 +v_0\int_0^L d^Dx\,d^Dx'\delta^d(\mathbf{r}(x)-\mathbf{r}(x')) . \tag{10}$$

The above discussion suggests that it might be possible to generalize Eq. (10) to include fractal networks by simply making the replacement $D\rightarrow d_S$. However, this does not work, as can be easily verified. For example, requiring the Gaussian part of $\beta\mathcal{H}(D\rightarrow d_S)$ to be scale invariant does not give the same result for $\nu$ as does Eq. (3). The reason for this failure is that whereas $\int d^Dx$ implies an integration over a homogeneous and compact space, $\int d^{d_S}x$ implies neither. Rather than attempt to discuss a measure theory for fractal sets, which would be needed to understand fully the meaning of $\int d^{d_S}x$, I will simply propose an ansatz for establishing a correspondence between a fractal manifold and an homogeneous one that has the same physics. The resulting Hamiltonian can then be analyzed in a straightforward manner.

The only other parameter besides $d_S$ that characterizes the internal space is $L$. It is not surprising that an intrinsic length scale might be modified for the case of a fractal manifold, since, unlike homogeneous networks, which are characterized by a single intrinsic large length scale $L$, fractals have many such scales, and it is not clear which scale is appropriate for integration. Assuming an in-

tegration scale of the form $L^x$, we can fix $x$ by requiring

$$\int_0^{L^x} d^{d_S}x = N \ , \tag{11}$$

from which we obtain $x = d_{fl}/d_S$. The Hamiltonian resulting from this correspondence,

$$\lim_{\substack{L\to L^{d_{fl}/d_S} \\ D\to d_S}} \beta\mathcal{H} = \beta\mathcal{H}'$$
$$= \int_0^{L^{d_{fl}/d_S}} d^{d_S}x \left[\frac{\partial \mathbf{r}(x)}{\partial x}\right]^2 + v_0 \int_0^{L^{d_{fl}/d_S}} d^{d_S}x \, d^{d_S}x' \times \delta^d(\mathbf{r}(x)-\mathbf{r}(x')) \ , \tag{12}$$

has the same upper-critical dimension and Gaussian scaling exponent as the original Sierpinski gasket model. It also leads to the same Flory theory prediction. For example, applying the usual Gaussian integration techniques[7] to the calculation of the mean-squared distance between two points of the phantom network gives

$$\langle [\mathbf{r}(x_1)-\mathbf{r}(x_2)]^2 \rangle = \frac{d\,\Gamma(\frac{1}{2}d_S)}{\pi^{d_S/2}(2-d_S)} |x_1-x_2|^{2-d_S} \ . \tag{13}$$

The rms end-to-end distance, which scales like $R_g$, is obtained by setting $|x_1-x_2| = L^{d_{fl}/d_S}$, from which we obtain a result identical to Eq. (3). Application of the usual power-counting arguments to Eq. (12) gives results identical to Eqs. (7) and (9). In addition, $\epsilon$-expansion results for $\nu$ can be obtained directly from the homogeneous-manifold results (cf. Ref. 17),

$$\nu_\epsilon = \nu_0 + \frac{d_{fl}}{d_S} \frac{(2-d_S^*)\epsilon}{8[d_S^* + 2C(d_S^*)]} + O(\epsilon^2) \ , \tag{14}$$

where

$$\epsilon = 4d_S - (2-d_S)d \ , \tag{15a}$$

$$C(d_S^*) \equiv \frac{\sqrt{\pi}\,\Gamma\left[\frac{2}{2-d_S^*}\right]}{2^{2d_S^*/(2-d_S^*)}\,\Gamma\left[\frac{2+d_S^*}{2(2-d_S^*)}\right]} \ , \tag{15b}$$

and

$$d_S^* = \frac{2d^*}{4+d^*} \ . \tag{15c}$$

The $\epsilon$ expansion is performed about the arbitrary point $(d_S^*, d^*)$, which lies on the critical line that separates SA-relevant behavior from SA-irrelevant behavior. If Eq. (14) turns out to be consistent with numerical results for the Sierpinski gasket (which, as we shall see, it does), then they provide evidence for the correctness of the ansatz, Eq. (12).

## III. SIMULATIONS

In order to perform Monte Carlo (MC) simulations, tethered-network versions of the Sierpinski gasket were developed.

(1) For the phantom network, all vertices are free to move through the embedding space subject only to the constraint $|\mathbf{r}^{(i)}-\mathbf{r}^{(j)}|2 \le 1$; $i$ and $j$ label connected nearest-neighbor vertices.

(2) For the self-avoiding network, an additional constraint is imposed: $\frac{1}{4} \le |\mathbf{r}^{(i)}-\mathbf{r}^{(j)}|2$; $i,j$ any two vertices of the network. In the ball-and-string language, the model uses strings of unit length and balls of diameter $\frac{1}{2}$.[18]

Temporal evolution of the simulations proceeds by a standard Metropolis algorithm. A vertex in the network is chosen at random and displaced by a random $d$-dimensional vector. If the trial move does not violate any of the applicable constraints, the move is accepted. $N$ such trial moves constitute a MC step of the network. A natural time scale (measured in MC steps) is the Rouse time,[1]

$$\tau_R = \frac{2\,dN}{\pi^2 s^2} \ , \tag{16}$$

where $s$ is the maximum length of the random-move vector. Since there is no intrinsic energy scale in either model, acceptance of a trial move is determined solely by the constraints, and in this sense the simulations were done at infinite temperature.

The simulations were started from a flat configuration, and data were taken every $\tau_R/10$ MC steps. The data consisted of the eigenvalues $\lambda_i$ $(i=1,\ldots,d;$ $\lambda_1 \le \lambda_2 \le \cdots \le \lambda_d)$ of the inertia tensor,

$$T_{ij} = \sum_{k=1}^{N} (r_i^{(k)} - r_{i,\mathrm{c.m.}})(r_j^{(k)} - r_{j,\mathrm{c.m.}}) \ , \tag{17}$$

where $r_i^{(k)}$ is the $i$th component of the $d$-dimensional position vector of the $k$th vertex. After a run of approximately $1000\tau_R$ each simulation was interrupted to determine the initial relaxation time, which was typically less than $100\tau_R$. The remaining data were then used to measure the relaxation time $\tau$ of the eigenvalue autocorrelation function,

$$\frac{1}{\tau} \equiv \lim_{t\to 0} \frac{-1}{t} \ln \left[ \frac{\langle R_g(t+t')R_g(t') - \langle R_g(t')\rangle^2 \rangle}{\langle [R_g(t') - \langle R_g(t')\rangle]^2 \rangle} \right] \tag{18}$$

($\langle\ \rangle$ denotes an average over the MC time $t'$ and is effectively an ensemble average). The simulation was then restarted and allowed to run until sufficient data had been acquired so that the statistical error in $R_g^2 (= \sum_i \lambda_i)$ was less than 1% at the $2\sigma$ level.

The measured eigenvalues were then used to calculate the scaling exponent,

$$\nu^{(n)} = d_{fl} \frac{\ln(R_g^{(n)}/R_g^{(n-1)})}{\ln(N^{(n)}/N^{(n-1)})} \ , \tag{19}$$

where $R_g^{(n)}$ and $N^{(n)}$ refer to the $n$th generation network values of $R_g$ and $N$, respectively. Calculating $\nu$ in this way makes the importance of any finite-size effects more evident than, say, a least-squares fit of all data points. However, it does lead to a larger error.

In order to determine whether or not the simulations

exhibit crumpling, we must, of course, have a reasonable definition of what constitutes a crumpled network. To do this, first consider the scaling exponents for the individual $\lambda_i$'s,

$$\nu_i = \lim_{n\to\infty} \nu_i^{(n)} , \tag{20a}$$

where

$$\nu_i^{(n)} = \frac{d_{fl} \ln(\lambda_i^{(n)}/\lambda_i^{(n-1)})}{2\ln(N^{(n)}/N^{(n-1)})} \tag{20b}$$

and $i=1,\ldots,d$. Note that $\nu=\nu_d$. Theoretical calculations to date have assumed the existence of two types of behavior: (1) flat, for which $\nu=\nu_d=\nu_{d-1}=1$ and $\nu_i<1$ for $i=1,\ldots,d-2$; (2) crumpled, for which $\nu=\nu_i<1$ for $i=1,\ldots,d$. There is, however, a third possibility, which has been observed in MC simulations:[4] (3) rough, for which $\nu=\nu_d=\nu_{d-1}<1$ and $\nu_i<\nu_d$ for $i=1,\ldots,d-2$.

If there were only the flat and crumpled regimes (as appears to be the case for SA homogeneous membranes embedded in $d=3$), then $\nu$ would be sufficient to determine which one was observed. However, since $\nu<1$ cannot distinguish between the rough and crumpled regimes, we must find some other test. In principle, the $\nu_i$'s could be used, but they are much more difficult to calculate theoretically or to measure from simulation data than $\nu$. This difficulty can be circumvented by introducing the shape parameter,

$$S_d = \lim_{n\to\infty} S_d^{(n)} , \tag{21a}$$

where

$$S_d^{(n)} = \left\langle \frac{\lambda_{d-2}^{(n)}}{\lambda_d^{(n)}} \right\rangle . \tag{21b}$$

$S_d^{(n)}$ is easy to measure from simulation data, although it might be quite difficult to calculate theoretically. Since $S_d\neq 0$ only in the crumpled regime, it can be used to distinguish between rough and crumpled behavior. The results of this discussion are summarized in Table I.

It is also worthwhile to measure another shape parameter,[19]

$$A_d = \lim_{n\to\infty} A_d^{(n)} , \tag{22a}$$

where

$$A_d^{(n)} = \frac{\sum_{\substack{i,j \\ i>j}} \langle (\lambda_i^{(n)} - \lambda_j^{(n)})^2 \rangle}{(d-1)\left\langle \left[\sum_i \lambda_i^{(n)}\right]^2 \right\rangle} , \tag{22b}$$

TABLE I. Criteria for determining the different regimes of a tethered network.

| Regime | $\nu$ | $S_d$ |
|---|---|---|
| Flat | 1 | 0 |
| Rough | $<1$ | 0 |
| Crumpled | $<1$ | $\neq 0$ |

which has been used in polymer studies. Although not very useful for determining whether a network is flat, rough, or crumpled, it does give a more detailed characterization of the shape than $S_d$. If all the $\lambda_i$'s are approximately equal, the crumpled configuration will be nearly spherical. The numerator of Eq. (22b) then will be small compared to the denominator, and $A_d\approx 0$. Conversely, if $\lambda_d$ is much larger than the other $\lambda_i$'s, the configuration will be "cigar shaped," and $A_d\approx 1$.

*Error analysis.* There are three important sources of error in the estimates of $R_g$: statistical-measurement errors, long-time-relaxation correlations, and finite-size effects.

The statistical error was determined by two different methods: (1) configurations temporally separated by $2.3\tau$ were treated as independent (i.e., correlations less than $e^{-2.3}\approx 0.01$ were ignored), and a simple error analysis based on the number of independent samples was done; and (2) a more sophisticated analysis was done,[20] which took into account the measured correlation between samples. Both methods gave similar error estimates, and in all cases the larger error estimate was used.

All of the data sets exhibit an initial rapid relaxation toward equilibrium followed by a much slower one. Typically, $R_g$ is within 2% of equilibrium after only $100\tau$, but to improve this by an order of magnitude requires a run of at least several thousand $\tau$. Removal of the effects of the initial relaxation was done by simply ignoring the first $100\tau$ of data. The effects of the long-term relaxation were more difficult to sort out since they were often about the same size as the statistical errors. Without a reliable method for estimating these effects, the only alternative was to increase the number of ignored initial data points. This both reduced the long-time-relaxation effects and increased the statistical errors; the latter eventually overwhelming the former. In practice, an initial cutoff was found acceptable if the remaining data, after binning, had an approximately Gaussian distribution.

Because the simulations were done for finite (and rather small) $n$, the data must be extrapolated to the $n\to\infty$ limit to obtain meaningful results. These effects, difficult to estimate without a finite-size scaling theory, are probably the most important. They were estimated by simply extrapolating the statistical errors from the two largest systems to the $n\to\infty$ limit. Examples of this method are the dotted lines in Figs. 3(a) and 3(b). Note that only the largest system was used to determine the lower error estimate for $\nu$ and $A_d$, and the upper error estimate for $S_d$. The rationale for this is the assumption that the slopes of the curves should not change sign. Hence, the single data point provides a realistic bound on the related estimate. Also note that the estimates for $\nu$, $S_d$, and $A_d$ have been chosen simply to be midway between their upper and lower error estimates.

## IV. RESULTS

*Phantom networks.* Figure 2 shows the results of simulations of phantom networks done for $d=3$ and $d=9$. To facilitate extrapolation of the data to the $n\to\infty$ limit, $\nu^{(n)}$, $S_d^{(n)}$, and $A_d^{(n)}$ have been plotted versus $1/n$. Also,

the $\nu^{(n)}$'s are plotted horizontally midway between the two relevant values of $n$. With the exception of the $n=5$, $d=3$ data point, the $\nu^{(n)}$'s are all consistent with the theoretical prediction for $\nu_0$ discussed in Sec. II, and they appear to be independent of $d$. The failure of this one point to fit the theory probably reflects the extremely long run time ($\gg 2800\tau$) needed to equilibrate the system satisfactorily. From the shape data, one can see that $S_d^{(n)}$ approaches a finite value in the $n\to\infty$ limit, indicating, as one would expect, that phantom networks crumple. Comparison of the $A_d$ results with the corresponding polymer values[19] ($A_3\approx 0.526$ and $A_9\approx 0.431$) shows that crumpled phantom Sierpinski gaskets are much more spherical than their polymer counterparts.

*Self-avoiding networks.* Figure 3 shows results for the $d=3$ SA network. The Flory prediction for $\nu$ is remarkably good—differing from the data by at most a few percent. This is consistent with the $d=2$ simulation of this model.[21] As with the phantom case, $S_d$ approaches a finite value for $n\to\infty$, indicating that the network is crumpled, although its much smaller value than the corresponding phantom one suggests that the SA network is much flatter in shape. This conclusion is also borne out, to some extent, by the $A_3$ data. This is different from polymers, where self-avoidance has almost no effect on $A_3$.[22] However, as $d$ increases, the distinction between the phantom and SA values for $A_d$ disappears.

Results for all the simulations are summarized in Table II and Fig. 4. Figure 4 shows that the data are consistent with the Flory theory for $d\leq 8$. The first-order $\epsilon$-expansion results are not as good for $d=3$, but improve, as one would expect, as $d\to d_{\rm UC}$. The data also show a clear crossover to Gaussian behavior in the $8\leq d\leq 10$ re-

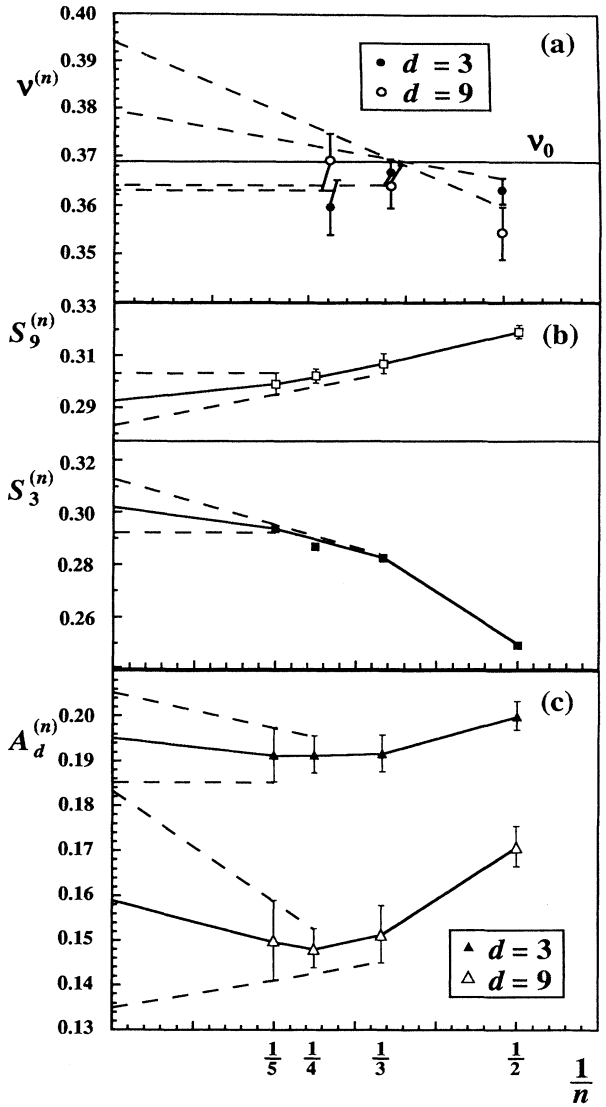


FIG. 2. Results for the phantom-network simulations. (a) $\nu^{(n)}$ vs $1/n$; the curves for extrapolating $\nu^{(n)}$ have been omitted for clarity; (b) $S_d^{(n)}$ vs $1/n$; (c) $A_d^{(n)}$ vs $1/n$. Error bars on all points reflect statistical errors only. Also note that the points in (a) have been positioned at $1/2\frac{1}{2}, 1/3\frac{1}{2}$, etc. to reflect the fact that they have been determined using the two simulations whose $n$ values they lie between.

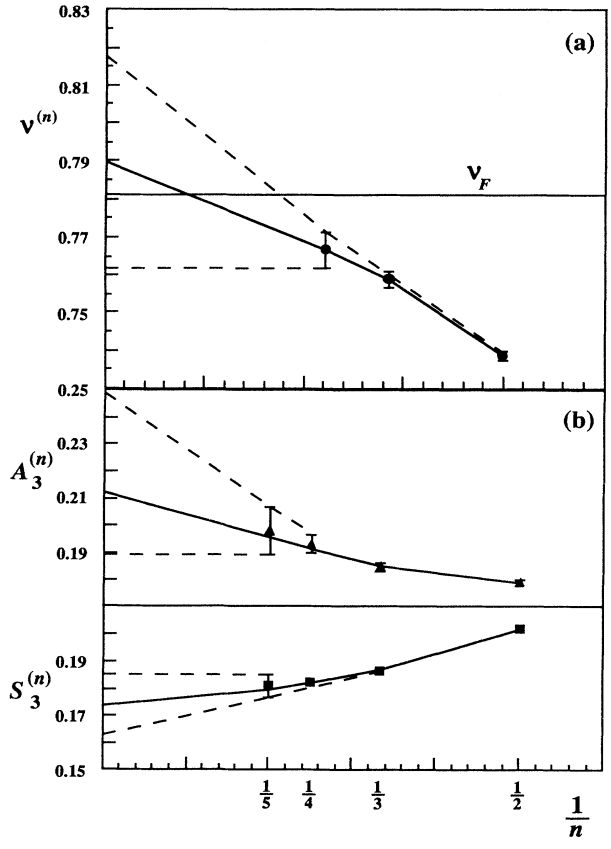


FIG. 3. Results for the $d=3$ SA-network simulations. (a) $\nu^{(n)}$ vs $1/n$; the Flory theory prediction is shown for comparison; (b) $S_d^{(n)}$, $A_d^{(n)}$ vs $1/n$. Error bars on all points reflect statistical errors only. The meaning of the dashed lines is explained in the error-analysis portion of Sec. III. Also note that the points in (a) have been positioned at $1/2\frac{1}{2}, 1/3\frac{1}{2}$, etc. to reflect the fact that they have been determined using the two simulations whose $n$ values they lie between.

TABLE II. Summary of simulation parameters and results. The run lengths do not include the initial discarded data. The quoted errors include both statistical and finite-size errors.

| Type | $d$ | Length of run (in $\tau$) $n=2$ | $n=3$ | $n=4$ | $n=5$ | $\nu$ | $S_d$ | $A_d$ |
|---|---|---|---|---|---|---|---|---|
| Phantom | 3 | 1452 | 1884 | 1808 | 1411 | 0.372±0.008 | 0.302±0.010 | 0.195±0.010 |
| | 9 | 87 | 79 | 232 | 67 | 0.379±0.016 | 0.292±0.010 | 0.159±0.024 |
| SA | 3 | 693 | 482 | 204 | 47 | 0.790±0.028 | 0.176±0.012 | 0.210±0.025 |
| | 7 | 523 | 709 | 163 | 18 | 0.451±0.019 | 0.295±0.018 | 0.177±0.022 |
| | 8 | 260 | 320 | 70 | 26 | 0.412±0.023 | 0.298±0.028 | 0.167±0.024 |
| | 9 | 442 | 557 | 280 | 17 | 0.395±0.018 | 0.291±0.011 | 0.172±0.032 |
| | 10 | 358 | 459 | 32 | | 0.382±0.016 | 0.283±0.013 | 0.143±0.017 |
| | 11 | 203 | 225 | 67 | | 0.361±0.007 | 0.289±0.006 | 0.133±0.010 |
| | 14 | 731 | 639 | 611 | | 0.380±0.016 | 0.272±0.013 | 0.131±0.007 |

gion. The exact location of the crossover is not very well determined, but it is certainly consistent with the prediction $d_{UC} \approx 8.6$.

There are several obvious extensions one could make to the present work, of which I mention only two. The first is to include bending energy in the simulation models and look for a crumpling transition. Currently, there are no known SA tethered-network models that exhibit a crumpling transition (they are either always flat or always crumpled), so it would, of course, be interesting to find a counter example. The second extension is to explore more fully the phase diagram in Fig. 5. Although not as interesting from a physical point of view as the corresponding diagram for homogeneous systems,[23] it does have the advantage that the $1 < d_S < 2$ region of the diagram is accessible to simulations, whereas the $1 < D < 2$ region of the homogeneous diagram is not. Furthermore, the results of this paper suggest that a correspondence between regular fractal manifolds and homogeneous ones may exist, although work remains to be done to justify the treatment of the Edwards model given here. This is important since theoretical analyses[2,9,10,17] of membranes have so far been unsuccessful in discovering the flat phase (but see Ref. 24). It may be possible, then, to set up a systematic program of simulations of regular fractal systems on the one hand, and theoretical calculations of the corresponding homogeneous manifolds on the other. One could then explore in detail their relationship to ques-

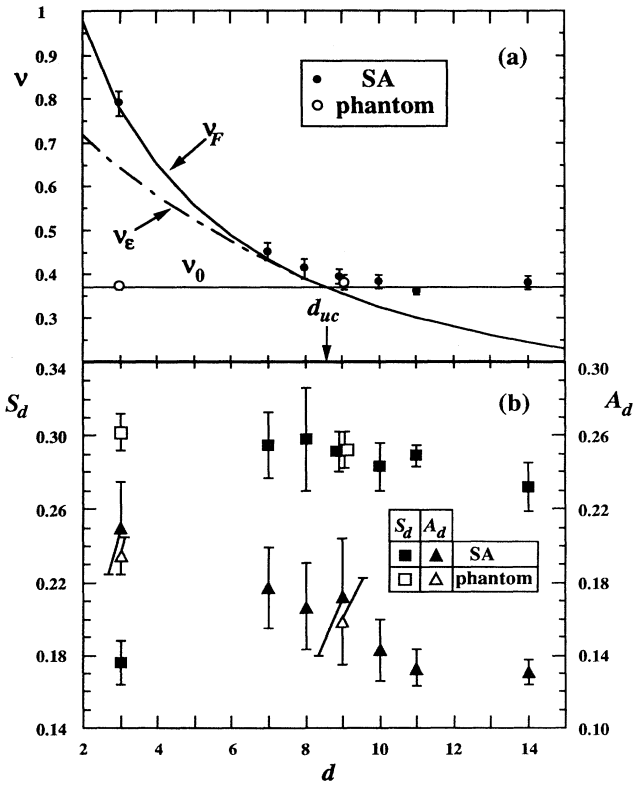


FIG. 4. Summary of all simulations done. (a) $\nu$ vs $d$. The Flory prediction ($\nu_F$), obtained from Eq. (7), and the $\epsilon$-expansion prediction ($\nu_\epsilon$), obtained from Eq. (14), are shown for comparison; (b) $S_d$, $A_d$ vs $d$. The error bars in both figures include finite-size effects as well as statistical errors.

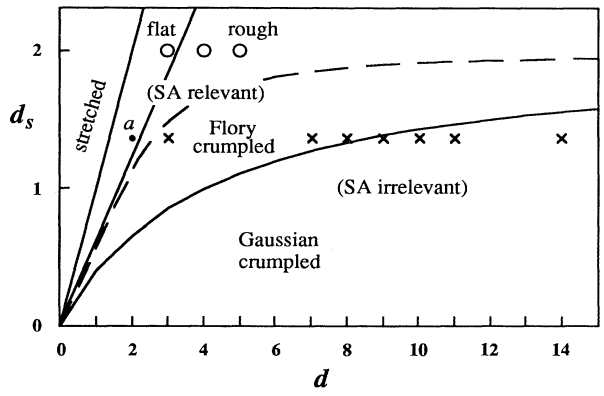


FIG. 5. Phase diagram for regularly connected fractal networks. The crosses represent the data from this simulation; the open circles are taken from Ref. 4. The dashed curve is hypothetical; although the point labeled $a$ (discussed in Ref. 21) is taken to be evidence for its existence. The precise location of the flat-rough boundary is also unknown.

tions concerning the existence of phase boundaries. For example, if a first-order phase boundary exists between the $D=2$ and SA-irrelevant lines, $\epsilon$ expansions will not detect it; but a corresponding boundary in the $d_S$-$d$ plane could be found through simulation. Indeed, one such phase boundary may have already been discovered.[21]

## ACKNOWLEDGMENTS

The author wishes to thank M. Wortis for many thoughtful conversations, M. Plischke for originally suggesting this work, Y. Kantor for helpful correspondence, and J. Glosli for assistance with the simulations.

---

*Electronic address: levinson @ whistler. sfu.ca (internet).

[1]Y. Kantor, M. Kardar, and D. R. Nelson, Phys. Rev. Lett. **57**, 791 (1986); Phys. Rev. A **35**, 3056 (1987); Y. Kantor and D. R. Nelson, *ibid.* **36**, 4020 (1987); M. Kardar and D. R. Nelson, *ibid.* **38**, 966 (1988).

[2]Y. Kantor, in *Statistical Mechanics of Membranes and Surfaces,* Proceedings of the Fifth Jerusalem Winter School, edited by D. R. Nelson, T. Piran, and S. Weinberg (World Scientific, Singapore, 1989), p. 115.

[3]S. Leibler and A. C. Maggs, Phys. Rev. Lett. **63**, 406 (1989).

[4]M. Plischke and D. Boal, Phys. Rev. A **38**, 4943 (1988); F. F. Abraham, W. E. Rudge, and M. Plischke, Phys. Rev. Lett. **62**, 1757 (1989); D. Boal, E. Levinson, D. Liu, and M. Plischke, Phys. Rev. A **40**, 3292 (1989).

[5]J.-S. Ho and A. Baumgartner, Phys. Rev. Lett. **63**, 1324 (1989).

[6]P. G. deGennes, *Scaling Concepts in Polymer Physics* (Cornell University Press, Ithaca, New York, 1979).

[7]J. des Cloizeaux, J. Phys. (Paris) **42**, 635 (1981).

[8]H. E. Stanley, P. J. Reynolds, S. Redner, and F. Family, in *Real-Space Renormalization,* edited by T. W. Burkhardt and J. M. J. van Leeuwen (Springer, New York, 1982), p. 169.

[9]E. Bouchard and J.-P. Bouchard, J. Phys. (Paris) **50**, 829 (1989).

[10]B. Duplantier, in *Statistical Mechanics of Membranes and Surfaces* (Ref. 2), p. 225.

[11]Some authors argue that this merely indicates the need to carry out the expansion to higher order to obtain sensible results.

[12]The assumption that $\nu<1$ implies crumpling seems to be appropriate only for $d=3$. A more general definition is given in Sec. III.

[13]A. Khurana, Phys. Today **42** (8), 17 (1989).

[14]The notion of the spectral dimension (sometimes referred to as the fracton dimension) of a network originally arose from the study of the density of states for a generalized Laplacian operator on a fractal. See S. Alexander and R. Orbach, J. Phys. (Paris) Lett. **43**, L-625 (1982) and R. Rammal and G. Toulouse, *ibid.* **44**, L-13 (1983) for this point of view. More recently, $d_S$ has been used to characterize random walks on fractal lattices, $\langle[\mathbf{r}(t)-\mathbf{r}(0)]^2\rangle \sim t^{d_S/d_{fl}}$. This will be used here as a definition of $d_S$. $d_{fl}$ is the fractal dimension of the lattice; i.e., $N \sim L^{d_{fl}}$, where $N$ is the number of vertices on the lattice. See M. Cates, J. Phys. (Paris) **46**, 1059 (1985); B. O'Shaunessy and I. Procaccia, Phys. Rev. A **32**, 3073 (1985); R. A. Guyer, *ibid.* **29**, 2751 (1984); and Ref. 15 for this latter point of view.

[15]J. A. Given and B. B. Mandelbrot, J. Phys. B **16**, L565 (1983).

[16]S. F. Edwards, Proc. Phys. Soc. London **85**, 613 (1965). A more modern view of this model can be found in Ref. 10.

[17]J. A. Aronovitz and T. C. Lubensky, Europhys. Lett. **4**, 395 (1987); B. Duplantier, Phys. Rev. Lett. **58**, 2733 (1987); M. Kardar and D. R. Nelson, Phys. Rev. A **38**, 966 (1988).

[18]Numerical studies done so far on tethered membrane models show no dependence of $\nu$ on the ratio of ball size to tether length. See F. F. Abraham, W. E. Rudge, and M. Plischke, Phys. Rev. Lett. **62**, 1757 (1989) and D. Boal, E. Levinson, D. Liu, and M. Plischke, Phys. Rev. A **40**, 3292 (1989). The choice made in the present work is dictated by computational convenience.

[19]J. Rudnick and G. Gaspari, Science **237**, 384 (1987).

[20]P. A. P. Moran, Biometrika **62**, 1 (1975).

[21]E. Duering and Y. Kantor, Phys. Rev. B **40**, 7443 (1989).

[22]J. A. Aronovitz and D. R. Nelson, J. Phys. (Paris) **47**, 1445 (1986).

[23]D. R. Nelson, in *Statistical Mechanics of Membranes and Surfaces* (Ref. 2), p. 1.

[24]T. Hwa, Phys. Rev. A **41**, 1751 (1990).